Quaternary Science Reviews 92 (2014) 123–132

Contents lists available at ScienceDirect

Quaternary Science Reviews

journal homepage: www.elsevier.com/locate/quascirev

Arctic Ocean perennial sea ice breakdown during the Early Holocene Insolation Maximum☆

Christian Stranne [a,*], Martin Jakobsson [b], Göran Björk [a]

[a] Department of Earth Sciences, University of Gothenburg, 413 20 Göteborg, Sweden
[b] Department of Geological Sciences, Stockholm University, 106 91 Stockholm, Sweden

ARTICLE INFO

Article history:
Received 15 February 2013
Received in revised form
1 October 2013
Accepted 20 October 2013
Available online 19 December 2013

Keywords:
Arctic climate
Holocene
Milankovitch cycles
Bølling–Allerød
Albedo feedback
Arctic sea ice

ABSTRACT

Arctic Ocean sea ice proxies generally suggest a reduction in sea ice during parts of the early and middle Holocene (~6000–10,000 years BP) compared to present day conditions. This sea ice minimum has been attributed to the northern hemisphere Early Holocene Insolation Maximum (EHIM) associated with Earth's orbital cycles. Here we investigate the transient effect of insolation variations during the final part of the last glaciation and the Holocene by means of continuous climate simulations with the coupled atmosphere–sea ice–ocean column model CCAM. We show that the increased insolation during EHIM has the potential to push the Arctic Ocean sea ice cover into a regime dominated by seasonal ice, i.e. ice free summers. The strong sea ice thickness response is caused by the positive sea ice albedo feedback. Studies of the GRIP ice cores and high latitude North Atlantic sediment cores show that the Bølling–Allerød period (c. 12,700–14,700 years BP) was a climatically unstable period in the northern high latitudes and we speculate that this instability may be linked to dual stability modes of the Arctic sea ice cover characterized by e.g. transitions between periods with and without perennial sea ice cover.

1. Introduction

Numerous palaeoclimate archives and numerical simulations suggest that the Arctic was warmer than present day during early and middle Holocene with peak air temperatures occurring at slightly different times in different regions (Kaufman et al., 2004; Renssen et al., 2012). While reconstructing paleo-sea ice extent from proxies is a challenging task (de Vernal et al., 2013), there are several independent studies of Arctic Ocean sea ice proxies suggesting that parts of this period was also characterized by less sea ice over large areas and potentially even sea ice free summers (e.g. Vare et al., 2009; Hanslik et al., 2010; Funder et al., 2011; Müller et al., 2012). The cause of this sea-ice minimum, occurring between about 6000 and 10,000 years BP, is often attributed to the northern hemisphere Early Holocene Insolation Maximum (EHIM) associated with Earth's orbital cycles (Jakobsson et al., 2010; Polyak et al., 2010; Müller et al., 2012). Insolation is in this context defined as the down-welling short wave (SW) radiation at the top of the atmosphere. Although the global mean insolation has been nearly constant during the Holocene, there have been significant latitudinal variations in insolation. These changes are mainly due to variations in two of Earth's orbital parameters: the obliquity and the precession (Berger, 1978). As a result, the annual mean insolation was around 5 Wm^{-2} larger at 80°N during the EHIM compared to present day conditions (Fig. 1a). However, due to the long polar night at this high latitude monthly averages of the insolation provide a clearer view of the actual variation of the insolation over time. For instance, the difference in mean June insolation is at 80°N about 50 Wm^{-2} between EHIM and present day (Fig. 1b). The radiative forcing from a doubling of the pre-industrial atmospheric CO_2 concentration has been estimated to ~3.5 Wm^{-2} (Gettelman et al., 2012). This is on the same order of magnitude as the increased SW forcing in the Arctic during the EHIM, although only a fraction of the insolation is available for melting ice due to the cloud and surface albedos.

The local Arctic climate system is an intimately coupled system between the ocean, the sea ice cover and the atmosphere. Its sensitivity to climate change is often investigated with coupled ocean–sea ice–atmosphere models. Previous studies have shown that detailed knowledge about the Arctic sea ice cover, and how it reacts to changes in external forcing, is critical when addressing the Arctic climate system as a whole and its variation during the Holocene (e.g. CAPE Project members, 2001). The climatic importance

* Corresponding author. Tel.: +46 31786 2874.
E-mail addresses: christian.stranne@gmail.com, christian.stranne@gvc.gu.se (C. Stranne).

0277-3791/$ – see front matter © 2013 The Authors. Published by Elsevier Ltd. All rights reserved.
http://dx.doi.org/10.1016/j.quascirev.2013.10.022

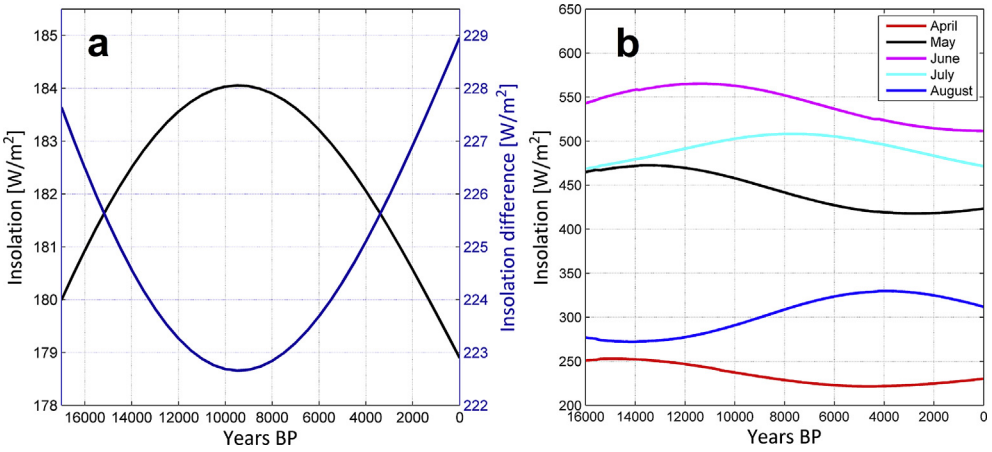

Fig. 1. Evolution of the insolation during the Holocene. A. The annual mean insolation at 80°N (*black curve*) and the annual mean insolation difference between 80°N and the equator (*blue curve*) with separate scale to the right. B. The monthly mean insolation at 80°N.

of the sea ice lies in the potentially large and sudden changes in the surface albedo which, through the sea ice albedo feedback, is one of the most important mechanisms for the Arctic energy budget (Curry et al., 1995; Houghton et al., 2001). The albedo feedback increases the Arctic climate system sensitivity drastically and is therefore vital to include in Arctic climate model simulations. Modelled sea-ice cover sensitivity itself is, however, sensitive to the details of the albedo parameterization as shown by Björk et al. (2012). This problem is a subject of further discussion in our present paper.

The Arctic sea ice response to the increased insolation during mid-Holocene (defined as 6000 years BP, i.e. 3500 years after the EHIM peak) has been investigated with atmospheric General Circulation Models (GCMs) (e.g. Harrison et al., 2002) and coupled ocean–atmosphere (and sometimes also vegetation) GCMs (e.g. Braconnot et al., 2007; Goosse et al., 2013). These simulations employ a time slice approach where the model spins up to steady state under prescribed mid-Holocene SW forcing. The general conclusion from studies within the Paleoclimate Modelling Intercomparison Project (PMIP) phase 1–3, is that a reduction of the Arctic sea-ice cover occurred during the mid-Holocene compared to pre-industrial conditions (Zhang et al., 2010). It should be noted, however, that there is a considerable spread in the PMIP results concerning how much the reduction in sea-ice cover was during the mid-Holocene. Transient simulations of the Arctic sea ice conditions during Holocene have been performed with Earth system models of intermediate complexity (Ganopolski et al., 1998a; Crucifix et al., 2002). However, none of the modelling efforts shows close to ice free summers (here referred to as seasonal ice) in the Arctic Ocean during the mid-Holocene.

Here we investigate the transient effect of insolation variations during the final part of the last glaciation and the Holocene by means of continuous climate simulations with the coupled atmosphere-ice-ocean column model CCAM (Stranne and Björk, 2011). We employ the simulations over time steps of 2 h. The results are compared to previously published modelling efforts and Arctic Ocean sea ice paleo records. Potential explanations for differences between our modelling results and previously published are discussed.

2. Methods

The Arctic sea ice conditions are simulated from the later part of the last Glacial Maximum (17,000 years BP) and throughout the Holocene using the coupled atmosphere–sea ice–ocean column model CCAM (Stranne and Björk, 2011). The atmospheric part of the CCAM is a standalone version of the column radiation code employed by the NCAR Community Climate Model (CCSM3) (Collins et al., 2006). It has a vertical grid comprised of 18 layers. A convective adjustment scheme and an internal heat source in each layer, corresponding to the external energy supply at the vertical boundary (F_{wall}), are added in the present application. The sea ice cover is separated into ~50 ice categories of different thicknesses, i.e. a sea ice thickness distribution. Each category may also have a snow cover on top (Björk, 1997). The ocean is represented by a column model with an active surface mixed layer controlled by mechanical mixing due to wind/ice motion and buoyancy fluxes at the surface. The stratification is also controlled by advective processes due to Bering Strait inflow (where Q_{bs}, S_{bs} and T_{bs} represents volume transport, temperature and salinity respectively), river discharge Q_f, geotropical outflow, and a hypothetical shelf circulation according to (Björk, 1989), see Table 1. The ocean/sea ice surface is coupled with the atmosphere such that heat fluxes are computed individually for each ice category, including open water. The single column atmosphere is updated using area weighted heat fluxes. The model is started at 19,100 years BP and runs continuously with a time step of 2 h until present (defined as year 2000 AD).

The algorithms for calculating the orbital parameters for a given year and for calculating the solar declination angle and the Earth/Sun distance factor for a given time of the year are based on the work presented by Berger (1978) and are valid as far back as one million years before present (BP). This algorithm is more accurate for years closer to present than the 10 million year solution of Berger and Loutre (1991). Atmospheric greenhouse gases are kept at pre-industrial levels during the whole simulations with methane, nitrous oxide and carbon dioxide concentrations of 0.715, 0.270 and 280 ppmv respectively (IPCC AR4). The atmospheric heat advection across the 70°N latitude circle (F_{wall}) follows an annual climatological cycle presented by Serreze et al. (2007) based on ERA-40 reanalysis data with a baseline annual mean F_{wall} of approximately 100 Wm^{-2} (Table 1). Clouds occupy a specific fraction, CF, of the sky at three different levels and follows an annual climatological cycle calculated from the ISCCP D2 dataset (Rossow and Duenas, 2004), Table 1. Climatological precipitation S_{prec} is calculated from the Arctic Meteorology and Climate Atlas (Arctic Climatology Project, 2000) where only area weighted ocean grid cells have been considered. The precipitation is tuned by a factor 1.5

Table 1
Model forcing and seasonal dependent parameters.[a]

	Jan	Feb	Mar	Apr	May	Jun	Jul	Aug	Sep	Oct	Nov	Dec
F_{wall} [W m^{-2}]	108	112	110	92	66	89	94	98	106	114	105	111
D [10^{-9} s^{-1}]	5.4	5.4	5.3	5.1	3.0	4.3	3.8	3.7	4.3	4.3	5.0	5.7
CF_{high}	0.08	0.09	0.06	0.02	0.01	0.02	0.04	0.04	0.04	0.04	0.05	0.07
CF_{mid}	0.50	0.50	0.49	0.34	0.22	0.25	0.29	0.32	0.34	0.37	0.44	0.49
CF_{low}	0.11	0.10	0.11	0.17	0.20	0.20	0.20	0.20	0.21	0.23	0.16	0.12
α_{snow}[b]	0.85	0.84	0.83	0.81	0.82	0.78	0.64	0.69	0.84	0.85	0.85	0.85
S_{prec} [mm/day]	1.0	0.9	0.9	0.7	0.7	0.9	1.4	1.6	1.6	1.4	1.1	1.0
Q_f 10^6 [m^{3}s^{-1}]	0.026	0.021	0.022	0.023	0.110	0.290	0.160	0.120	0.094	0.063	0.031	0.026
Q_{be} 10^6 [m^{3}s^{-1}]	1.02	0.95	0.34	0.78	1.13	1.26	1.47	1.07	0.66	0.87	0.90	0.34
S_{be}	32.2	32.6	32.7	32.6	32.3	32.2	32.4	32.1	32.0	31.6	31.5	31.7
T_{be} [°C]	−1.7	−1.8	−1.8	−1.8	−1.2	0.8	3.8	4.3	4.2	3.1	−1.2	−1.7

[a] For additional parameters see Björk and Soderkvist (2002).
[b] Annual cycle of snow albedo in the Maykut surface albedo parameterization.

so that the annual maximum snow depth equals 0.3 m under present day baseline forcing. The ice export follows a prescribed annual cycle and is described by the divergence parameter D taken from Kwok and Rothrock (1999), Table 1. The simulated pre-industrial seasonal cycles for a selection of model state variables are shown in Fig. 2.

3. Results

3.1. Model results

Three main simulations were carried out. In the first simulation the sea ice albedo feedback was switched off by pre-setting a constant surface albedo (= 0.68) regardless of surface type. In the two subsequent simulations the albedo feedback was activated through the use of a dynamic surface albedo parameterization dependent on the surface type and ice thickness (Maykut, 1982, see Appendix 1 for details). Since the Arctic sea ice cover is subject to a hysteresis when transitioning between seasonal and perennial ice, a third reversed simulation was carried out where the model was run from present day conditions and backwards in time in terms of SW forcing.

With constant albedo the annual mean sea ice thickness at EHIM is reduced by about 0.7 m compared to the present day pre-industrial thickness of 3 m (Fig. 3a). When using a dynamic surface albedo parameterization the reduction becomes considerably larger. The sea ice cover then enters a regime with ice free summers between about 6000 and 11,700 years BP (Fig. 3b). The sudden transitions from a perennial to a seasonal ice cover at 11,700 years BP and from a seasonal to a perennial ice cover at 6000 years BP are related to the fact that there is no stable state in the model characterized by a brief ice free period in the summer; it is either perennial sea ice or ice free conditions for an extended period of time in the summer. As explained in detail in Björk et al. (2012), the ice thickness distribution will more and more lean towards a dominant ice thickness category as the climate gets warmer. As soon as the dominating ice thickness category melts completely there is no possibility to maintain an equilibrium cycle with just a few days of open water because when this large area fraction becomes ice free the albedo will be lowered significantly and this enhances the amount of solar radiation absorbed by the ocean. The dominating ice thickness category will then melt somewhat earlier in the following summer season which will further enhance the oceanic absorption and so on. The system has then to find a new equilibrium characterized by a quite long period of almost completely open water during summer (a few thick ridged ice categories will still survive the summer but these occupy only a very small area fraction). This process is often referred to as the surface albedo feedback. Similar transitions between perennial and seasonal sea ice conditions in the Arctic due to the surface albedo feedback can be found also in GCM simulations (Holland et al., 2006). Below we will refer to this process as sea ice albedo

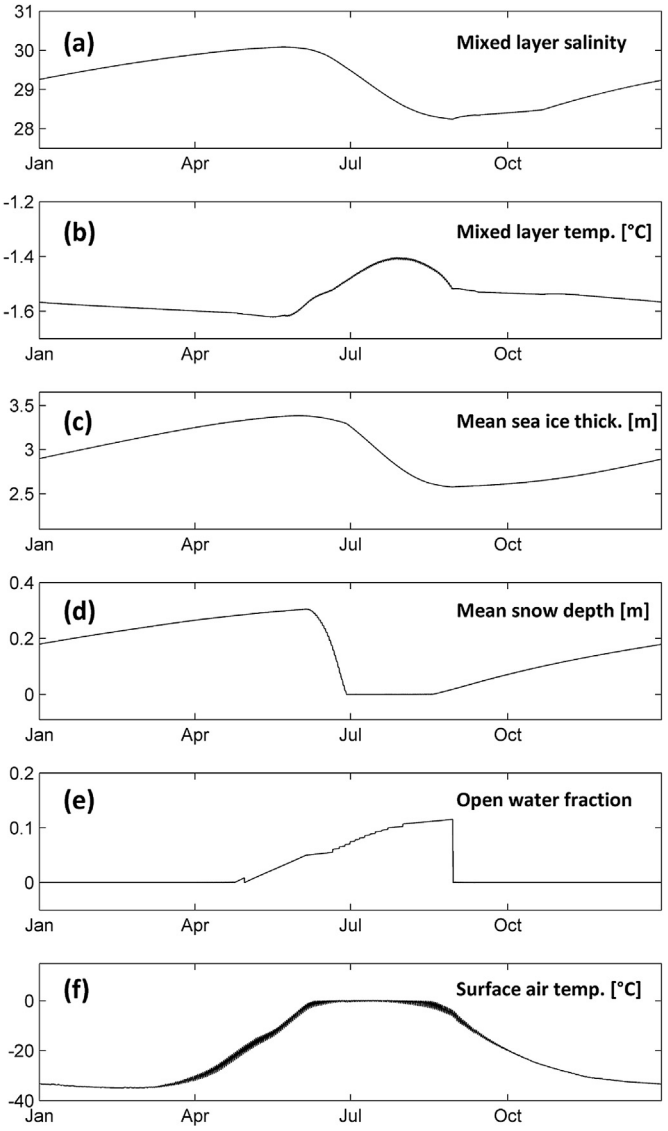

Fig. 2. CCAM simulated seasonal cycles for a selection of ocean (a–b), sea ice (c–e) and atmosphere (f) model variables under pre-industrial forcing (see Table 1 for details).

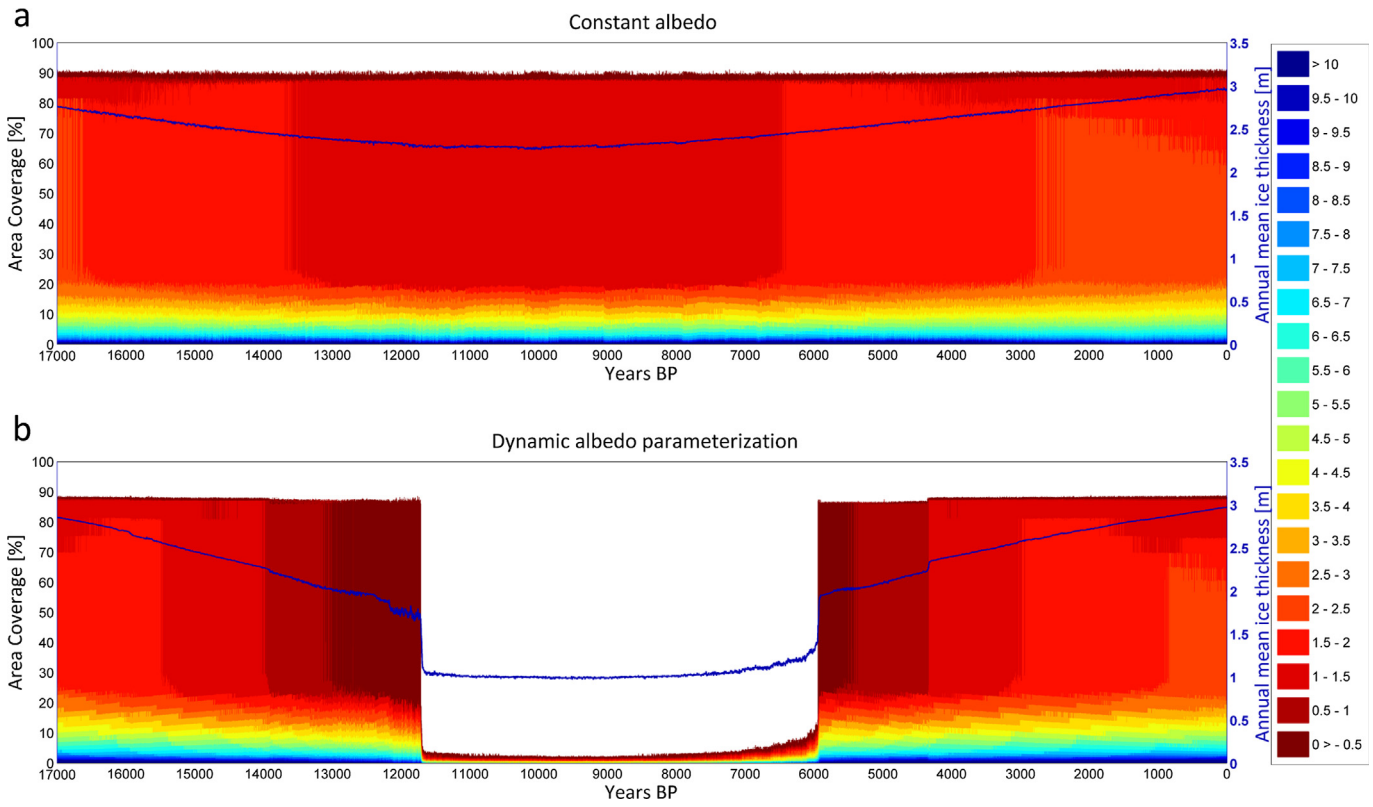

Fig. 3. Simulated area coverage of different ice thickness categories in the Arctic Ocean at the time of the maximum open water area fraction each year for a) constant surface albedo b) dynamic surface albedo parameterization (see Appendix for details). White indicates the open water fraction. The blue line shows the simulated annual mean sea ice thickness with a separate scale to the right.

feedback to distinguish it from the surface albedo feedback associated with vegetation.

Whether or not there is an irreversible tipping point associated with the transition between perennial and seasonal ice has been discussed recently (Stranne and Björk, 2011; Tietsche et al., 2011). The mechanism behind such a critical threshold involves a combination of sea ice albedo feedback and the large heat storage capacity of the ocean. Following a change from colder to warmer climate in the Arctic, the feedback from a reduced albedo due to less sea ice will eventually kick in, leading to a rapid transition of the sea ice cover into a state dominated by seasonal ice. At this point the oceanic heat storage increases drastically, which in turn implies that the climate must return to a colder state compared to when the transition originally occurred in order to force the ice cover back into a perennial state. Consequently, there is a range in the forcing with two stable modes depending on the initial state of the sea ice cover which is hereafter referred to as a hysteresis. The hysteresis of the Arctic sea ice cover is here investigated through a reversed simulation where the model is run from present day conditions and backwards in time in terms of SW forcing. Comparing the annual mean sea ice thickness between the two simulations clearly shows the hysteresis (Fig. 4a). The hysteresis is small in terms of forcing (<1 Wm^{-2}, Fig. 5) which is actually smaller than the typical present day interannual variability of the thermodynamic forcing itself. For comparison we calculated the standard deviation of the annual mean atmospheric heat advection across the 70°N latitude circle (F_{wall}) between 1954 and 2000 to $\sim$5 Wm^{-2} using data from the National Centers for Environmental Prediction (NCEP) reanalysis data product, and the methods of Overland and Turet (1994). The small hysteresis is consistent with the results of Tietsche et al. (2011) and Stranne and Björk (2011) and is a consequence of the highly effective ocean–atmosphere heat transfer during autumn and winter under ice free conditions. Even though the hysteresis is small in terms of forcing, it is relatively long in terms of time (c. 1000 years) due to the slow gradual changes in the SW forcing (Fig. 4a). In our simulations, a hysteresis is covering the mid-Holocene (defined as 6000 years BP in the PMIP), meaning that the state of the modelled ice cover is a function of the initial conditions during this period of time. The hysteresis is discussed in Section 4 in relation to Arctic climate proxy data and the climatically unstable Bølling–Allerød period.

3.2. Comparison between simulation results and paleo-sea ice records

Studies of Arctic Ocean sea ice variability extending in time beyond the satellite imagery record available since 1979 (Stroeve et al., 2011) have been carried out using paleo-proxies that provide information about past sea ice conditions. Adding recent results from paleo-sea ice studies to the syntheses by Jakobsson et al. (2010) and Polyak et al. (2010) seem to further support the view that generally less sea ice prevailed in the Arctic Ocean before approximately 6000 years BP (Fig. 4b). For example, using abundance and origin of drift wood and beach ridges (indicating wave activity) Funder et al. (2011) infer a multiyear sea ice minimum along the coast of Northern Greenland between $\sim$8500 and 6000 years BP, with a limit of a perennial sea ice about 1000 km north of its present position. In the Fram Strait between Greenland and Svalbard, a sea ice minimum is evident in sediment cores from variations of the sea ice proxy IP_{25} (Müller et al., 2012). However, this minimum appears to have occurred somewhat earlier, at about 6500 years BP.

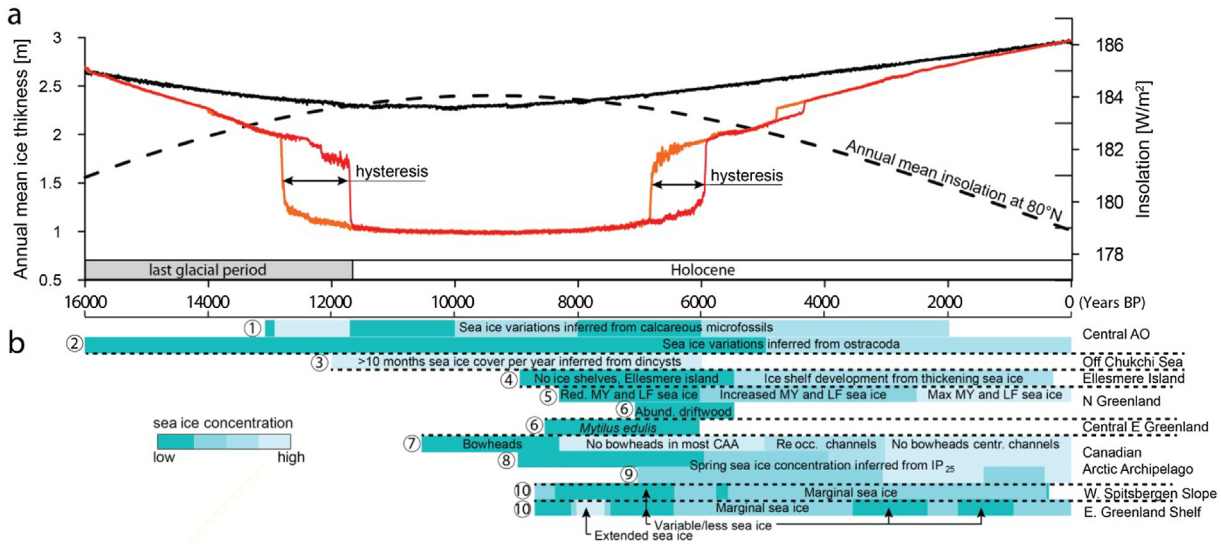

Fig. 4. Annual mean sea ice thickness for the three different simulations (Panel a) compared with results from published paleo-sea ice studies (Panel b). Black curve: constant surface albedo; red curve: dynamic surface albedo parameterization. The simulation implemented with a dynamic surface albedo parameterization was run from present time and backwards to address the importance of the initial state of the sea ice cover. The annual mean sea ice thickness from this simulation (orange curve) reveals a hysteresis of ~1000 years. The annual mean insolation at 80°N shown with a stippled curve is based on the algorithm presented by Berger (1978). To compare the results from different paleo-sea ice studies a scale of sea ice concentration was inferred using the approach by Jakobsson et al. (2010). This scale must be considered as highly qualitative because none of the paleo-sea ice proxies provide absolute measures of past sea ice concentrations. The number preceding each bar representing the result of a paleo-sea ice study corresponds to the following references: 1: Hanslik et al. (2010); 2: Cronin et al. (2010); 3: de Vernal et al. (2005); 4: England et al. (2008); 5: Funder et al. (2011); 6: Bennike (2004); 7: Dyke et al. (1996); 8: Vare et al. (2009); 9: Belt et al. (2010); 10: Müller et al. (2012). MY = Multi Year; LF = Land Fast Ice.

Whether or not the summer sea ice disappeared in the Holocene over the entire Arctic Ocean is far from resolved from paleo-proxies, although the majority of published results seems to indicate a substantial decrease in the earlier and middle part of the Holocene (Fig. 4b). Contradicting results exists for example from the western Arctic Ocean where dinosyst assemblages in a sediment core suggest a more extensive sea ice cover, than at present, between 12,000 and 6000 years BP (de Vernal et al., 2005), Fig. 4b. Similarly to the modelling intercomparison projects (e.g. PMIP), the sea ice paleo-proxy community has now begun systematic comparisons between different proxies (de Vernal et al., 2013). Already, important inconsistencies between the applied proxies are high-lighted.

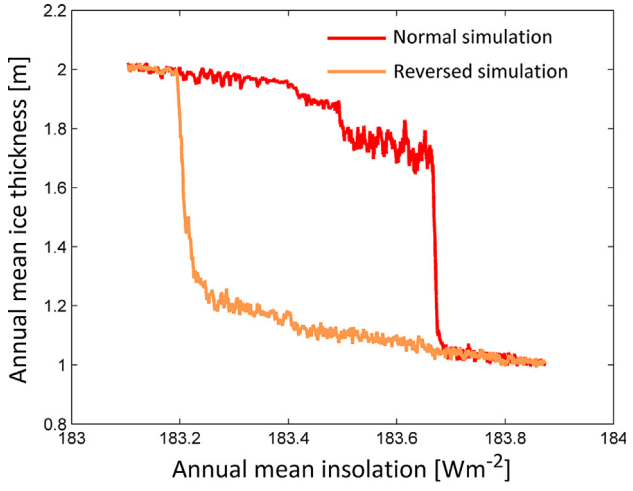

Fig. 5. The hysteresis in terms of SW forcing is shown by plotting the annual mean ice thickness against annual mean insolation at the top the atmosphere over the period 11,000–13,000 years BP for the normal simulation (red curve) and the reversed simulation (orange curve).

4. Discussion

The present idealized model study focuses on the isolated effect of variations in the SW forcing during Holocene by means of transient simulations performed with a coupled ocean–sea ice–atmosphere column model. Our simulations yield a period during early and mid-Holocene dominated by seasonal ice, indicating a potentially large impact of the EHIM on the sea ice cover through the sea ice albedo feedback. The breakdown of the perennial sea ice cover is however a feature not seen in other model studies of mid-Holocene Arctic sea ice conditions e.g. in the PMIP simulations (Harrison et al., 2002; Braconnot et al., 2007; Goosse et al., 2013). The reason behind the differences when comparing this study to previous modelling efforts can be due to several factors discussed below.

4.1. The transient versus the time slice modelling approach

One obvious reason for the large response of the ice cover in the present model compared to other modelling efforts under mid-Holocene forcing is that we are considering the entire Holocene including the 9500 years BP EHIM. Most previous studies, including the PMIP simulations, are performed with SW forcing corresponding to 6000 years BP conditions with an enhanced annual mean SW forcing in the Arctic of about 4 Wm^{-2} compared to about 5 Wm^{-2} during the EHIM (Fig. 1a). In the present model the ice cover is at the threshold between perennial and seasonal sea ice conditions for SW forcing corresponding to 6000 years BP. The transient simulation by Crucifix et al. (2002) performed with an Earth system model of intermediate complexity between 9000 years BP to present shows an Arctic climate which is peaking in terms of sea surface temperature, open water area etc. at the beginning of the simulation (9000 years BP) followed by a gradually colder climate towards present time. If the same model was run from the EHIM (9500 years BP) it would likely have started with a further reduced ice cover.

4.2. Feedback processes

It is generally believed that feedback processes within the climate system are of importance when simulating past, present and future climate. If a process increases (decreases) the sensitivity of the simulated climate compared to when it is not included in the model code, this process is here defined as a positive (negative) feedback. For instance, if the climate for some reason experiences a warming perturbation it is often assumed that the atmospheric water vapour content will increase. Since water vapour is a potent greenhouse gas the increase would then raise the temperature further and thus giving rise to even higher atmospheric water vapour contents and so on, until a new equilibrium is reached. This is an example of a positive feedback in the climate system which acts on a global scale, although the strength seems to vary with latitude (Bitz et al., 2012). There are many feedback processes, both negative and positive, in the global coupled climate system that need to be simulated accurately and in a physically realistic manner in order to assess climate sensitivity. Since feedback processes may be active on both regional and global scales and over a wide spectrum of time scales, they are sometimes problematic to represent in climate models and are often difficult verify. Both regional and global climate models are struggling to reproduce the observed sea ice retreat in the Arctic Ocean over the last four decades. Feedback processes associated with clouds, water vapour and sea ice have been identified as key mechanisms for explaining the discrepancy between observed and modelled climate change in the Arctic region (Holland et al., 2010). Berger et al. (2013) showed that an analytical one-equation thermodynamic model, developed by Thorndike (1992), is able to reproduce the sea ice sensitivity simulated by the general circulation models participating in the PMIP2 and PIMP3 projects fairly well. This is a surprising result since many of the feedbacks that are generally believed to be important e.g. feedbacks associated with surface albedo, ice dynamics and clouds are absent in the model. Their result implies that the Arctic sea ice cover sensitivity is controlled by its thermodynamic properties alone which is in stark contrast to the more established idea that climatic feedback processes on both regional and global scales are important for the Arctic sea ice sensitivity (e.g. Lesins et al., 2012; Morrison et al., 2012). An analysis of Thorndikes analytical model presented by Stranne and Björk et al. (2011) showed however that by just adding ice export to the model equation, the model sea ice sensitivity was drastically changed, a result that was also verified with the CCAM model (their Fig. 1c).

Climate simulations of the Arctic sea ice cover (both global and regional) have shown large inter-model scatter and analyses of the reason behind the spread in model results point at the surface albedo parameterization as one of the major factors (Wyser et al., 2008; Holland et al., 2010). This is because variations in the snow/ice albedo is one of the dominating factors influencing the Arctic energy budget i.e. the surface albedo can for a given area change drastically from bright fresh snow albedo (reflecting ~90% of the incoming SW radiation) to dark open ocean albedo (reflecting ~10% of the incoming SW radiation) in matter of weeks. This is the mechanism responsible for the sudden transitions between seasonal and perennial sea ice (Fig. 3b) which is discussed in more detail in Section 3.1.

There are however feedback mechanisms associated with local processes such as lapse rate, clouds, water vapour, snow precipitation as well as large scale processes associated with e.g. vegetation albedo, ocean circulation and atmospheric circulation that are not included in the present model. The net effect of these feedbacks, and possibly other more intricate mechanisms linked with e.g. methane release from thawing Siberian shelf sediments and tundra, are not yet fully understood. Although the feedback associated with atmospheric water vapour content is believed to be positive (Bitz et al., 2012) there are large uncertainties associated with simulating Arctic clouds (e.g. Wyser et al., 2008) and there is no consensus in the research community regarding whether the net effect of the cloud feedbacks is positive or negative (Cai and Lu, 2010).

Global scale studies of the surface albedo feedback associated with vegetation indicate that this is a strong positive feedback mechanism (Ganopolski et al., 1998a; Crucifix et al., 2002; Colleoni et al., 2009). Crucifix et al. (2002) show that the warmer conditions in the northern hemisphere during mid-Holocene caused a northward shift of the northern tree line compared to present day conditions. The resulting albedo effect from this vegetation change generated a doubling of the sea ice reduction compared to model simulations with fixed terrestrial surface albedo for the mid-Holocene, a result that is in qualitative agreement with the PMIP simulations (Braconnot et al., 2007). More recent climate simulations performed by Miller et al. (2010) confirm that indeed the vegetation feedback is positive in terms of albedo at high latitudes, but closer to the equator or in a significantly warmer climate the vegetation albedo feedback can become negative if evergreen forests are replaced by deciduous forests.

Variations in the SW forcing can also cause changes in the large scale atmospheric circulation patterns which in turn may affect the Arctic sea ice cover. For example, changes in wind driven ice export or changes in the meridional atmospheric heat advection into the Arctic (F_{wall}) may occur. Crucifix et al. (2002) show that F_{wall} was not significantly different during the mid-Holocene compared to present day conditions. A study by Kay et al. (2012) indicate that F_{wall} is slightly reduced under $2 \times CO_2$ GCM simulations (indicating a weak negative feedback) and argue that local feedbacks are more important than the coupling to the global climate system. Results from e.g. $2 \times CO_2$ experiments are however not directly comparable to this study where we look at insolation variations on multi-millennial time scales rather than increased GHG forcing on much shorter time scales. The variation in SW forcing over the Arctic region during the Holocene is slow and associated with a redistribution of the insolation (over seasons and over latitudes) rather than a global net forcing perturbation as in the $2 \times CO_2$ scenario. This means that when the insolation in the northern high latitudes increases during the EHIM, the insolation in other regions of the globe decreases. The difference in the annual mean insolation between the Arctic and the Equator and its variation during Holocene is shown in Fig. 1a which illustrates that the meridional insolation gradient reaches a minimum during the EHIM. Since F_{wall} is linked to the meridional insolation gradient (Stone and Miller, 1980) one would expect a smaller F_{wall} during the EHIM, which in turn would reduce the effect of the increased SW forcing on the Arctic Ocean sea ice thickness.

Previous climate simulations indicate a weakening of the Meridional Overturning Circulation (MOC) during mid-Holocene which acts as a negative feedback on the northern hemisphere and thus dampens the effect of the EHIM (Ganopolski et al., 1998b). Anderson et al. (2004) showed however in a study based on sediment core analyses that the North Atlantic Drift (NAD), which is the major current that transports warm and salty Atlantic surface water into the Arctic Ocean through Fram Strait (Rudels et al., 2012), was stronger during the mid-Holocene. The weakening of the MOC might then be compensated by the increased NAD in terms of oceanic heat advection into the Arctic. Joos et al. (1999) speculate that a weakened MOC can lead to a reduction in CO_2 enriched deep water formation and thus reducing the oceanic CO_2 uptake. A weakening of the MOC would then promote global warming and in a sense counteract the local effect.

4.3. External forcing

Variations of the atmospheric greenhouse gas (GHG) concentrations are not simulated in our baseline simulations presented in Fig. 3a where pre-industrial methane (CH_4), nitrous oxide (N_2O) and carbon dioxide (CO_2) concentrations in the atmosphere of 0.715, 0.270 and 280 ppmv (IPCC AR4), respectively are applied. The CCAM is run with constant atmospheric CO_2 concentrations in our baseline simulation for consistency with the PMIP projects where pre-industrial CO2 levels for the mid-Holocene time slice simulations are also applied. Several studies suggest that the GHG concentrations were lower during the EHIM (Indermuhle, 1999; Brook et al., 2000; Sowers et al., 2003). However, when running the model with GHG concentrations estimated from paleo-proxy data (LeGrande and Schmidt, 2009) for 9000 years BP yields only a moderate effect on the ice cover thickness of typically ~0.1 m, Fig. 6. This is consistent with the results of CAPE Project members (2001) showing also only marginal effects of the GHG concentration variations on the Arctic climate. The period dominated by seasonal ice is however reduced by more than 1500 years, indicating a large uncertainty in the timing of the modelled perennial sea ice cover breakdown, Fig. 6. This large uncertainty of the timing of the perennial sea ice breakdown is a direct effect of the extremely small rate of change in the SW forcing ($\sim 5 \times 10^{-4}$ W m^{-2} year^{-1}) in combination with the inherent forcing threshold of the modelled system, associated with the surface albedo feedback. Since GCMs can yield similar ice cover threshold behaviour to increased forcing (e.g. Holland et al., 2006) an analogous uncertainty would likely show up in such GCM simulations i.e. an uncertainty of the forcing threshold of 0.5 Wm^{-2} gives an uncertainty of the transition timing of around plus minus 1000 years.

4.4. Regional forcing variations

In the present column model approach the Arctic Ocean ice conditions are simulated using a spatially averaged forcing. In reality all forcing parameters have regional variations within the Arctic. In a GCM the forcing threshold between perennial and seasonal ice regimes will depend on location e.g. the region close to the North Pole has lower insolation compared to regions further south and would thus need a larger positive forcing perturbation before the sea ice albedo feedback sets in. For this reason the sharp transition between the seasonal and perennial ice cover regimes as shown in the present study would be less sharp (or sudden) when horizontal averages from GCM outputs are calculated. Holland et al. (2006) showed however that the surface albedo induced transition between the perennial and seasonal ice cover regimes in the Arctic indeed can be seen clearly also in GCM simulations.

4.5. Model formulations and parameterizations

Different model formulations and their representation of physical processes can influence the response properties of the modelled sea ice cover. This is evident when considering the inter-model scatter in terms of Arctic sea ice response in the PMIP project (e.g. Zhang et al., 2010). Although there are several possible explanations to the spread between model results in terms of Arctic sea ice conditions (Goosse et al., 2013), numerous studies have pointed out variations in the albedo parameterization as one of the major factors (e.g. Wyser et al., 2008; Holland et al., 2010). The sensitivity of the Arctic sea ice cover response properties to changes in the albedo parameterization is here exemplified by performing the same experiment as in the baseline model run but with the CSIRO Mk3 albedo parameterization (Gordon et al., 2002, see Appendix for details). The model now yields a much longer period of seasonal ice, again indicating a large uncertainty regarding the timing of the modelled perennial sea ice cover breakdown as discussed above, c.f. Fig. 3 and Fig. A1.

4.6. Hysteresis

In our simulations, a hysteresis is covering the mid-Holocene (defined as 6000 years BP in the PMIP), meaning that the state of the modelled ice cover is a function of the initial conditions during this period of time. This might also be a feature of GCM models included in the PMIP simulations. However, since the hysteresis is smaller than the natural interannual variability of the forcing, evidence from such hysteresis should in a GCM (if the forcing variability is correctly reproduced by the model) show up as increased variability of the system where the ice cover fluctuates between the two stable modes rather than an initial condition dependent ice thickness as is the case here. If however the hysteresis is larger in a fully coupled system than in our column model, the initial conditions for the PMIP time slice simulations for mid-Holocene might still be of importance. As mentioned, a large variability of the ice cover can be expected over the periods

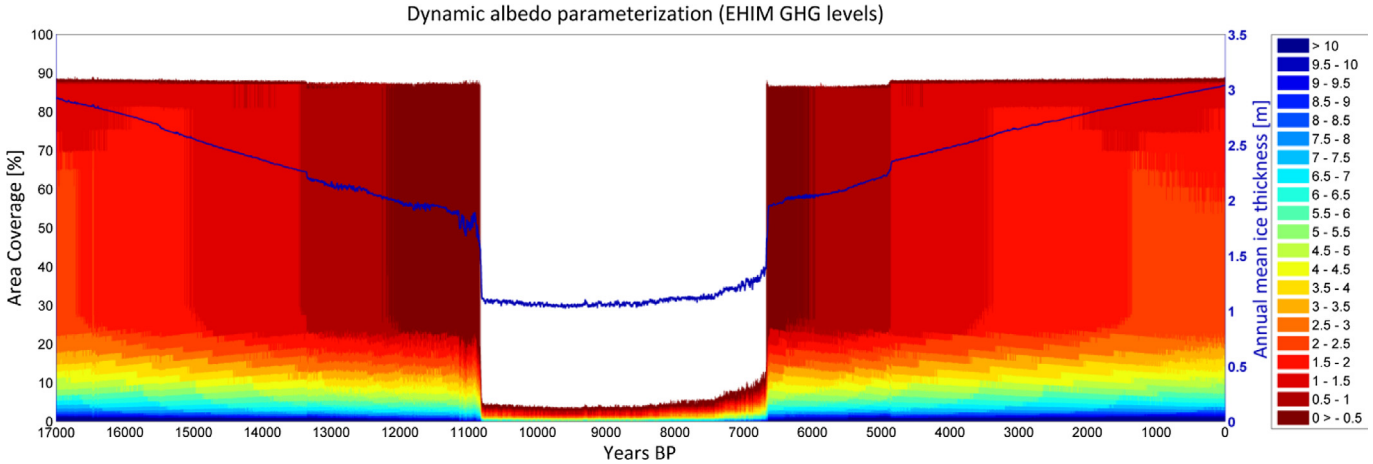

Fig. 6. Same as Fig. 2b but with constant GHG levels estimated for 9000 years BP, taken from (LeGrande & Schmidt, 2009). The seasonal ice period is reduced to about 4100 years compared to about 5700 years when the model is forced with constant preindustrial GHG levels.

with dual equilibria during which the ice cover can switch easily between perennial and seasonal ice on relative short decadal to interannual time scales. Stranne and Björk (2011) showed that the Arctic sea ice cover is likely subject to a similar but significantly larger hysteresis associated with a sudden blocking of the Arctic Ocean sea ice export passages when the mean sea ice thickness reaches a certain threshold, a phenomenon known as sea ice arching (Hibler et al., 2006). We speculate that such dual stability modes can explain periods dominated by large variability in the Arctic Ocean climate system e.g. the climatically unstable Bølling–Allerød period ~12,700–14,700 years BP (Koc et al., 1996; Rasmussen, 2006).

4.7. Further aspects

Other factors of potential importance for the sea ice cover not considered in our simulations include changes in the freshwater supply and variations in sea level. Since the cloud and water vapour dynamics of the Arctic atmosphere is not well understood snow precipitation is difficult to model accurately (e.g. Verlinde et al., 2007; Soden and Held, 2006) and it is hard to validate the model output due to the scarce observational precipitation data available for the central Arctic. Changes in snow precipitation in the Arctic area would not only influence the fresh water budget but would also alter the surface albedo which in turn affects the Arctic sea ice sensitivity as was shown by Björk et al. (2012). Factors like the persistence of e.g. the Laurentide ice sheet until 8000 years BP (Hughes et al., 1981; Lambeck et al., 2000) probably had an impact on the Arctic climate through effects associated with both freshwater supply and surface albedo.

The present study points at a potentially large impact of the increased SW forcing during EHIM through the surface albedo feedback, leading to a breakdown of the perennial sea ice cover into a state dominated by ice free summers. Above we have discussed some mechanisms and feedback processes that are not included in the present model study. Although some of the in this model omitted mechanisms are believed to be important (e.g. the surface albedo feedback associated with vegetation) the current understanding of the climate system as a whole is far from complete. Evidence of problems with the coupled GCMs can be found in the PMIP literature. For instance Jiang et al. (2012) show that 35 out of 36 PMIP models produce colder than present day climate in China during mid-Holocene which is in stark contrast to available multiproxy data for the same time and region indicating 1–5 °C warmer than present day conditions. In another study Zhang et al. (2010) compared the two best PMIP models in terms of northern high latitude climate proxy data agreement for the mid-Holocene (the FOAM and the MRI models). They show that even between the two best models there are significant inter-model differences. During the melt season the FOAM (MRI) model produced e.g. a sea ice area fraction reduction of 8 (25) %, a sea ice thickness reduction of 0.8 (1.5) m and a surface heat flux increase of 4 (22) Wm^{-2} compared to present day pre-industrial conditions. Suffice to say that further research on the coupled global climate system is needed before any conclusive results regarding the evolution of the Arctic sea ice cover during Holocene can be reached through climate modelling.

5. Conclusions

Based on the observed Arctic Ocean sea ice decline during the recent decades we know that the climate system is sensitive to changes in the external forcing. The recent decline has proved to exceed several estimates from coupled general circulation model studies (Stroeve et al., 2007) and from this notion alone one could argue that it seems highly plausible that the sea ice cover was reduced compared to present day pre-industrial conditions also during early and middle Holocene as a consequence of the EHIM. This study shows that the EHIM has the potential to force the Arctic sea ice cover into a regime dominated by seasonal ice. These results provides a similar view as the interpretation of available Arctic sea ice paleo-proxy data (Fig. 4b). Our work points to the strong surface albedo feedback as the common denominator between the sea ice minimum before 6000 years ago and the present diminishing trend. However, at the same time as our simulations show the importance of the surface albedo feedback, there are likely two distinctly different underlying causes for the feedback to kick in: increased insolation (past) and increased GHG levels (present). We also speculate that climatically unstable periods such as the Bølling–Allerød period (c. 12,700–14,700 years BP) can be explained by dual stability modes of the Arctic sea ice cover associated with e.g. the transition between perennial and seasonal sea ice conditions.

Acknowledgements

This work was funded by the EU project DAMOCLES (contract 018509), the Swedish Research Council (contract 621-2007-3836) and the Research Platform TELLUS at University of Gothenburg. The contribution by M. Jakobsson was supported by the Knut and Alice Wallenberg Foundation (the SWERUS-C3 project), the Swedish Research Council (grant 2008-2843) and forms a contribution from the Bolin Centre for Climate Research.

Appendix 1. Albedo parameterizations

Maykut albedo parameterization

The dynamic albedo parameterization is a function of surface type i.e. open water, bare sea ice or snow covered, and sea ice thickness and is taken from Maykut (1982). The snow albedo follows a prescribed annual cycle (Table 1). The bare ice albedo α is a function of ice thickness following

$$\alpha = \min\left(0.08 + 0.44 h_{\mathrm{ice}}^{0.28}, 0.64\right)$$

which also gives the open water albedo for $h_{\mathrm{ice}} = 0$.

CSIRO Mk3 albedo parameterization

The CSIRO Mk3 albedo parameterization (Gordon et al., 2002) is a function of surface type i.e. open water, bare sea ice or snow covered sea ice, surface temperature, and solar zenith angle *zr*.

The open water albedo is a function of solar zenith angle:

$$\alpha = 0.05/(0.15 + abs(\cos(zr)))$$

For bare ice:

$$\alpha = \begin{cases} 0.65, & T_s < 0 \\ 0.55, & T_s \geq 0 \end{cases}$$

and for snow covered ice:

$$\alpha = \begin{cases} 0.80, & T_s < 0 \\ 0.70, & T_s \geq 0 \end{cases}$$

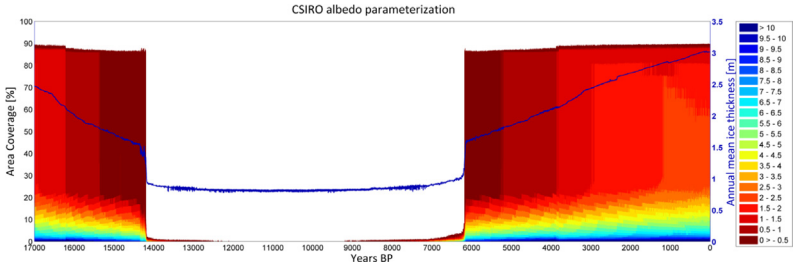

Fig. A1. Same as Fig. 2b in the main text but with a different type of albedo parameterization taken from the general circulation model CSIRO Mk3. Here we get a seasonal ice period of about 8000 years compared to about 5700 years when using the Maykut albedo (c.f. Fig. 2b).

References

Anderson, C., Koç, N., Moros, M., 2004. A highly unstable Holocene climate in the subpolar North Atlantic: evidence from diatoms. Q. Sci. Rev. 23, 2155–2166.

Arctic Climatology Project, 2000. In: Fetterer, F., Radionov, V. (Eds.), Environmental Working Group Arctic Meteorology and Climate Atlas. National Snow and Ice Data Center, Boulder.

Belt, S.T., et al., 2010. Striking similarities in temporal changes to spring sea ice occurrence across the central Canadian Arctic Archipelago over the last 7,000 years. Q. Sci. Rev. 29, 3489–3504.

Bennike, O., 2004. Holocene sea-ice variations in Greenland: onshore evidence. Holocene 14, 607–613.

Berger, A., 1978. Long-term variations of daily insolation and Quaternary climatic changes. J. Atmos. Sci 35, 2362–2367.

Berger, A., Loutre, M.F., 1991. Insolation values for the climate of the last 10 million of years. Q. Sci. Rev. 10, 297–317.

Berger, M., Brandefelt, J., Nilsson, J., 2013. The sensitivity of the Arctic sea ice to orbitally induced insolation changes: a study of the mid-Holocene Paleoclimate Modelling Intercomparison Project 2 and 3 simulations. Clim. Past 9, 969–982. http://dx.doi.org/10.5194/cp-9-969-2013.

Bitz, C.M., Shell, K.M., Gent, P.R., Bailey, D.A., Danabasoglu, G., Armour, K.C., Holland, M.M., Kiehl, J.T., 2012. Climate sensitivity of the community climate system model, version 4. J. Clim. 25, 3053–3070. http://dx.doi.org/10.1175/JCLI-D-11-00290.1.

Björk, G., 1989. A one-dimensional time-dependent model for the vertical stratification of the upper Arctic Ocean. J. Phys. Oceanogr. 19, 52–67.

Björk, G., 1997. The relation between ice deformation, oceanic heat flux, and the ice thickness distribution in the Arctic Ocean. J. Geophys. Res. Ocean. 102, 18681–18698.

Björk, G., Soderkvist, J., 2002. Dependence of the Arctic Ocean ice thickness distribution on the poleward energy flux in the atmosphere. J. Geophys. Res. Ocean. 107 (C10). http://dx.doi.org/10.1029/2000JC000723.

Björk, G., Stranne, C., Borenäs, K., 2013. The sensitivity of the Arctic Ocean sea ice thickness and its dependence on the surface albedo parameterization. J. Clim. 26, 1355–1370. http://dx.doi.org/10.1175/JCLI-D-12-00085.1.

Braconnot, P., et al., 2007. Results of PMIP2 coupled simulations of the Mid-Holocene and Last Glacial Maximum – Part 1: experiments and large-scale features. Clim. Past 3, 261–277. http://dx.doi.org/10.5194/cp-3-261-2007.

Brook, E.J., Harder, S., Severinghaus, J.P., Steig, E.J., Sucher, C.M., 2000. On the origin and timing of rapid changes in atmospheric methane during the Last Glacial period. Global Biogeochem. Cycl. 14, 559–572.

Cai, M., Lu, J.H., 2010. Quantifying contributions to polar warming amplification in an idealized coupled general circulation model. Clim. Dyn. 34 (5), 669–687. http://dx.doi.org/10.1007/s00382-009-0673-x.

CAPE Project members, 2001. Holocene paleoclimate data from the Arctic: testing models of global climate change. Q. Sci. Rev. 20, 1275–1287.

Colleoni, F., Krinner, G., Jakobsson, M., 2009. Sensitivity of the Late Saalian (140 kyrs BP) and LGM (21 kyrs BP) Eurasian ice sheet surface mass balance to vegetation feedbacks. Geophys. Res. Lett. 36, L08704.

Collins, W.D., et al., 2006. The formulation and atmospheric simulation of the community atmosphere model version 3 (CAM3). J. Clim. 19, 2144–2161.

Cronin, T.M., et al., 2010. Quaternary Sea-ice history in the Arctic Ocean based on a new Ostracode sea-ice proxy. Q. Sci. Rev. 29, 3415–3429.

Crucifix, M., Loutre, M.F., Tulkens, P., Fichefet, T., Berger, A., 2002. Climate evolution during the Holocene: a study with an Earth System model of intermediate complexity. Clim. Dyn. 19, 43–60.

Curry, J.A., Schramm, J.L., Ebert, E.E., 1995. On the sea ice albedo climate feedback mechanism. J. Clim. 8, 240–247.

de Vernal, A., Hillaire-Marcel, C., Darby, D., 2005. Variability of sea ice cover in the Chukchi Sea (western Arctic Ocean) during the Holocene. Paleoceanography 20, PA4018.

de Vernal, A., Gersonde, R., Goosse, H., Seidenkrantz, M.-S., Wolff, E.W., 2013. Sea ice in the paleoclimate system: the challenge of reconstructing sea ice from proxies – an introduction. Q. Sci. Rev. 79, 1–8. http://dx.doi.org/10.1016/j.quascirev.2013.08.009.

Dyke, A.S., Hooper, J., Savelle, J.M.A., 1996. History of sea ice in the Canadian arctic Archipelago based on Postglacial remains of the Bowhead Whale (Balaena mysticetus). Arctic 49, 235–255.

England, J.H., et al., 2008. A millennial-scale record of Arctic Ocean sea ice variability and the demise of the Ellesmere Island ice shelves. Geophys. Res. Lett. 35, L19502.

Funder, S., et al., 2011. A 10,000-year record of arctic ocean sea-ice variability—view from the beach. Science 333, 747–750.

Ganopolski, A., Kubatzki, C., Claussen, M., Brovkin, V., Petoukhov, V., 1998a. The influence of vegetation-atmosphere–ocean interaction on climate during the mid-Holocene. Science 280, 1916–1919.

Ganopolski, A., Rahmstorf, S., Petoukhov, V., Claussen, M., 1998b. Simulation of modern and glacial climates with a coupled global model of intermediate complexity. Nature 371, 323–326.

Gettelman, A., Kay, J.E., Shell, K.M., 2012. The evolution of climate sensitivity and climate feedbacks in the community atmosphere model. J. Clim. 25, 1453–1469.

Goosse, H., Roche, D.M., Mairesse, A., Berger, M., 2013. Modelling past sea ice changes. Q. Sci. Rev. 79, 191–206.

Gordon, H.B., et al., 2002. The CSIRO Mk3 Climate System Model. Technical Paper No. 60. CSIRO Atmospheric Research, Aspendale, Victoria, Australia.

Hanslik, D., et al., 2010. Quaternary Arctic Ocean sea ice variations and radiocarbon reservoir age corrections. Q. Sci. Rev. 29, 3430–3441.

Harrison, S., Braconnot, P., Hewitt, C., Stouffer, R.J., 2002. Fourth International Workshop of the palaeoclimate modelling intercomparison project (PMIP): launching PMIP phase Ii. EOS 83, 447.

Hibler, W.D., Hutchings, J.K., Ip, C.F., 2006. Sea-ice arching and multiple flow states of Arctic pack ice. Ann. Glaciol. 44, 339–344.

Holland, M.M., Bitz, C.M., Tremblay, B., 2006. Future abrupt reductions in the summer Arctic sea ice. Geophys. Res. Lett. 33, L23503. http://dx.doi.org/10.1029/2006GL028024.

Holland, M.M., Serreze, M.C., Stroeve, J., 2010. The sea ice mass budget of the Arctic and its future change as simulated by coupled climate models. Clim. Dyn. 34, 185–200. http://dx.doi.org/10.1007/s00382-008-0493-4.

Houghton, J.T., Ding, Y., Griggs, D.J., Noguer, M., Van der Linden, P.J., Dai, X., 2001. Climate Change 2001: The Scientific Basis. Cambridge, University Press, Cambridge.

Hughes, T.J., Denton, G.H., Andersen, B.G., Schilling, D.H., Fastook, J.L., Lingle, C.S., 1981. The last great ice sheets: a global view. In: Denton, G.H., Hughes, T.J. (Eds.), The Last Great Ice Sheets. J. Wiley & Sons, New York, pp. 263–317, 484.

Indermuhle, A., 1999. Holocene carbon-cycle dynamics based on CO2 trapped in ice at Taylor Dome, Antarctica. Nature 398, 121–126.

Jakobsson, M., Long, A., Ingólfsson, Ó., Kjær, K.H., Spielhagen, R.F., 2010. New insights on Arctic Quaternary climate variability from palaeo-records and numerical modeling. Q. Sci. Rev. 29, 3349–3358.

Jiang, D., Xianmei, L., Zhiping, T., Tao, W., 2012. Considerable model-data mismatch in temperature over China during the Mid-Holocene: results of PMIP Simulations. J. Clim. 25, 4135–4153. http://dx.doi.org/10.1175/JCLI-D-11-00231.1.

Joos, F., Plattner, G.-K., Stocker, T.F., Marchal, O., Schmittner, A., 1999. Global warming and marine carbon cycle feedbacks on future atmospheric CO_2. Science 284, 464–467.

Kaufman, D.S., et al., 2004. Holocene thermal maximum in the western Arctic (0–180°W). Q. Sci. Rev. 23, 23.

Kay, J., et al., 2012. The influence of local feedbacks and northward heat transport on the equilibrium Arctic climate response to increased greenhouse gas forcing. J. Clim. 25, 5433–5450.

Koc, N., Jansen, E., Jald, M., Labeyrie, L., 1996. Late glacial-Holocene sea surface temperatures and gradients between the North Atlantic and the Norwegian Sea: implications for the Nordic heat pump. In: Late Quaternary Palaoceanography of the North Atlantic Margins, vol. 111Geological Society Special Publication, pp. 177–185.

Kwok, R., Rothrock, D.A., 1999. Variability of fram strait ice flux and North Atlantic Oscillation. J. Geophys. Res. Ocean. 104, 23615.

Lambeck, K., Yokoyama, Y., Johnston, P., Purcell, A., 2000. Global ice volumes at the Last Glacial Maximum and early Lateglacial. Earth Planet. Sci. Lett. 181, 513–527.

LeGrande, A.N., Schmidt, G.A., 2009. Sources of Holocene variability of oxygen isotopes in paleoclimate archives. Clim. Past 5, 441–455.

Lesins, Glen, Duck, Thomas J., Drummond, James R., 2012. Surface energy balance framework for arctic amplification of climate change. J. Clim. 25, 8277–8288. http://dx.doi.org/10.1175/JCLI-D-11-00711.1.

Maykut, G.A., 1982. Large-scale heat-exchange and ice production in the central arctic. J. Geophys. Res. Ocean Atmos. 87, 7971–7974.
Miller, G.H., Alley, R.B., Brigham-Grette, J., Fitzpatrick, J.J., Polyak, L., Serreze, M., White, J.W.C., 2010. Arctic amplification: can the past constrain the future? Q. Sci. Rev. 29, 1779–1790.
Morrison, H., de Boer, G., Feingold, G., Harrington, J., Shupe, M., Sulia, K., 2012. Resilience of persistent Arctic mixed-phase clouds. Nat. Geosci. 5, 11–17. http://dx.doi.org/10.1038/ngeo1332.
Müller, J., et al., 2012. Holocene cooling culminates in sea ice oscillations in Fram Strait. Q. Sci. Rev. 47, 1–14.
Overland, J.E., Turet, P., 1994. Variability of the atmospheric energy flux across 70_N computed from the GFDL data set. In: Johannessen, O.M., Muench, R.D., Overland, J.E. (Eds.), The Polar Oceans and Their Role in Shaping the Global Environment, Geophysical Monograph Series, vol. 85, pp. 313–325.
Polyak, L., et al., 2010. History of sea ice in the Arctic. Q. Sci. Rev. 29, 1757–1778.
Rasmussen, S.O., 2006. A new Greenland ice core chronology for the last glacial termination. J. Geophys. Res. 111, D06102. http://dx.doi.org/10.1029/2005JD006079.
Renssen, H., Seppä, H., Crosta, X., Goosse, H., Roche, D.M., 2012. Global characterization of the Holocene thermal maximum. Q. Sci. Rev. 48, 7–19.
Rossow, W.B., Duenas, E.N., 2004. The International satellite cloud climatology project (ISCCP) web site—an online resource for research. Bull. Am. Meteorol. Soc. 85, 167–172.
Rudels, B., Anderson, L., Eriksson, P., Fahrbach, E., Jakobsson, M.,E.,P.J., Melling, H., Prinsenberg, S., Schauer, U., Yao, T., 2012. Observations in the Ocean. In: Lemke, P. (Ed.), Arctic Climate Change: The ACSYS Decade and Beyond. Springer, pp. 117–198.
Serreze, M.C., et al., 2007. The large-scale energy budget of the arctic. J. Geophys. Res. 112, D11122.
Soden, B.J., Held, I.M., 2006. An assessment of climate feedbacks in coupled ocean–atmosphere models. J. Clim. 19, 3354–3360.
Sowers, T., Alley, R.B., Jubenville, J., 2003. Ice core records of atmospheric N_2O covering the last 106,000 years. Science 301 (5635), 945–948.
Stone, P.H., Miller, D.A., 1980. Empirical relations between seasonal changes in meridional temperature gradients and meridional fluxes of heat. J. Atmos. Sci. 37, 1708–1721.
Stranne, C., Björk, G., 2011. On the Arctic Ocean ice thickness response to changes in the external forcing. Clim. Dyn. 39, 3007–3018. http://dx.doi.org/10.1007/s00382-011-1275-y.
Stroeve, J., Holland, M.M., Meier, W., Scambos, T., Serreze, M., 2007. Arctic sea ice decline: faster than forecast. Geophys. Res. Lett. 34, L09501.
Stroeve, J.C., et al., 2011. Sea ice response to an extreme negative phase of the Arctic Oscillation during winter 2009/2010. Geophys. Res. Lett. 38, L02502.
Thorndike, A.S., 1992. A toy model linking atmospheric thermalradiation and sea ice growth. J. Geophys. Res. Ocean. 97 (C6), 9401–9410.
Tietsche, S., Notz, D., Jungclaus, J.H., Marotzke, J., 2011. Recovery mechanisms of Arctic summer sea ice. J. Geophys. Res. Lett. 38, L02707.
Vare, L.L., Massé, G., Gregory, T.R., Smart, C.W., Belt, S.T., 2009. Sea ice variations in the central Canadian Arctic Archipelago during the Holocene. Q. Sci. Rev. 28, 1354–1366.
Verlinde, J., et al., 2007. The mixed-phase Arctic cloud experiment. Bull. Am. Meteorol. Soc. 88, 205–221. http://dx.doi.org/10.1175/Bams-88-2-205.
Wyser, K., et al., 2008. An evaluation of Arctic cloud and radiation processes during the SHEBA year: simulation results from eight Arctic regional climate models. Clim. Dyn. 30, 203–222. http://dx.doi.org/10.1007/s00382-007-0286-1.
Zhang, Q., Sundqvist, H.S., Moberg, A., Körnich, H., Nilsson, J., Holmgren, K., 2010. Climate change between the mid and late Holocene in northern high latitudes – Part 2: model-data comparisons. Clim. Past 6, 609–626. http://dx.doi.org/10.5194/cp-6-609-2010.